PAPER

High-Accuracy Estimation of Image Rotation Using 1D Phase-Only Correlation

Sei NAGASHIMA[†a)], ***Student Member***, **Koichi ITO**[†b)], **Takafumi AOKI**[†], ***Members***, **Hideaki ISHII**[††], ***Nonmember***, ***and*** **Koji KOBAYASHI**[††], ***Member***

SUMMARY This paper presents a technique for high-accuracy estimation of image rotation using 1D Phase-Only Correlation (POC). The rotation angle between two images is estimated as follows: (i) compute the amplitude spectra of the given images, (ii) transform the coordinate system of amplitude spectra from Cartesian coordinates to polar coordinates, and (iii) estimate the translational displacement between the polar-mapped amplitude spectra to obtain the rotation angle. While the conventional approach is to employ 2D POC for high-accuracy displacement estimation in (iii), this paper proposes the use of 1D POC with an adaptive line selection scheme. The proposed technique makes possible to improve the accuracy of rotation estimation for low contrast images of artificial objects with regular geometric shapes and to reduce the total computation cost by 50%.

key words: *image registration, rotation estimation, phase correlation*

1. Introduction

High-accuracy image registration is an important fundamental task in many fields, such as image sensing, image/video processing, computer vision, industrial image recognition, etc. Over the years, various techniques for image registration have been developed. Typical examples include image-correlation-based methods, Fourier-transform-based methods, image-feature-based methods, and others [1], [2]. Among many methods, image registration techniques using Phase-Only Correlation (POC) (or simply "phase correlation") have attracted much attention due to their high accuracy and robust performance. The POC-based approach for image registration is originally proposed for translated images [3], and its principle is extended to the registration of translated and rotated images [4] (with Euclidean transformation model) and also to the translated, rotated and scaled images [5] (with similarity transformation model).

In our previous work [6], we have proposed a set of techniques that can significantly enhance the accuracy of POC-based image registration. Using the proposed techniques, we can estimate translational image shift with 1/100-pixel accuracy, image rotation with 1/40-degree accuracy and image scaling with 1/10000-scale accuracy when the image size is 251×251 pixels [6]. These high-accuracy image registration techniques have been successfully applied to practical vision sensors [7] for industrial image recognition, where a specially designed ASIC processor is employed for high-speed computation of POC [8].

In many industrial applications, such as component alignment systems and chip mounters, high-accuracy estimation of rotation angles (with translational image shifts) is of fundamental importance. In typical situation of industrial machine vision, we can assume that the working distance of image sensing is fixed, which means that the captured images include only translations and rotations and do not include scale changes. Hence, the major task of image registration is to estimate image shift and image rotation simultaneously. A problem arises when we employ low contrast images of artificial objects with regular geometric shapes. Since such images contain only limited effective components in their amplitude spectra, the accuracy of rotation estimation degrades significantly.

Addressing this problem, this paper proposes an improved technique for estimating image rotation (with image shift) using 1D POC. The rotation angle between two images is estimated as follows: (i) compute the amplitude spectra of the given images, (ii) transform the coordinate system of the amplitude spectra from Cartesian coordinates (x, y) to polar coordinates (ρ, ϕ), and (iii) estimate the translational displacement between the polar-mapped amplitude spectra to obtain the rotation angle. While the conventional approach is to employ 2D POC for displacement estimation in (iii), this paper proposes the use of 1D POC with an adaptive line selection scheme.

Given a reference image, the system first selects a set of effective lines in its polar-mapped amplitude spectrum. Then, the 1D POC is computed for the selected lines to obtain the rotation angle. The proposed technique makes possible to improve the accuracy of rotation estimation for low contrast images of artificial objects. Also, the use of 1D POC instead of 2D POC allows us to reduce the computation cost by 50%, which leads to significant performance improvements for actual vision sensors.

Original contribution of this paper are summarized as follows: (i) estimating the image rotation angle using 1D POC instead of 2D POC, (ii) proposal of an adaptive line selection scheme that can find reliable image lines so as to improve the accuracy of rotation estimation, and (iii) systematic experimental evaluation of rotation estimation performance using actual images captured by a commercial-

Manuscript received September 28, 2007.
Manuscript revised March 8, 2008.

[†]The authors are with the Department of Computer and Mathematical Sciences, Graduate School of Information Sciences, Tohoku University, Sendai-shi, 980-8579 Japan.
[††]The authors are with Yamatake Corporation, Fujisawa-shi, 251-8522 Japan.
a) E-mail: nagasima@aoki.ecei.tohoku.ac.jp
b) E-mail: ito@aoki.ecei.tohoku.ac.jp

DOI: 10.1587/transfun.E92.A.235

off-the-shelf CCD camera.

This paper is organized as follows: Sect. 2 gives the fundamentals of image rotation estimation. In Sect. 3, we define the 1D POC function and present an improved rotation estimation algorithm using 1D POC. Section 4 presents a set of experiments for evaluating the accuracy of rotation estimation. In Sect. 5, we end with some conclusions.

2. Fundamentals of Image Rotation Estimation

This section introduces the principle of rotation estimation using 2D POC (Phase-Only Correlation) [4], [6]. The problem considered here is to estimate the rotation angle θ between two images that are translated and rotated with respect to each other. The first step is to separate the rotation from translation. The amplitude spectra of the original images are useful for this purpose. The amplitude spectra in 2D DFT are not affected by the translational image shifts. Instead, they are rotated with respect to each other at the origin of spatial frequency (the DC component) by the same angle as their spatial domain counterparts.

The next step is to convert the problem of rotation estimation into translation estimation by transforming the coordinate system of amplitude spectra from Cartesian coordinates (x, y) to polar coordinates (ρ, ϕ). Then, we estimate the translational displacement between the polar-mapped amplitude spectra to obtain the estimate $\hat{\theta}$ of the true rotation angle θ.

We can summarize the procedure of rotation estimation as follows.

Inputs:

- the reference image I to be registered in the system
- the image J for which the rotation angle should be estimated with respect to the reference image I

Output:

- the estimated rotation angle $\hat{\theta}$ of J with respect to I

Step 1:

Calculate the 2D DFT amplitude spectra of I and J (Fig. 1(a)) to have I_A and J_A (Fig. 1(b)), respectively.

Step 2:

For natural images, most energy is concentrated in low-frequency domain as shown in Fig. 1(b). Hence, we had better use the modified amplitude spectra $I_{LA} = \log(I_A + 1)$ and $J_{LA} = \log(J_A + 1)$ for rotation estimation. This enhances small-amplitude components in high frequency domain, while suppressing large-amplitude components in low frequency domain as shown in Fig. 1(c).

Step 3:

Transform the coordinate system of the modified amplitude spectra I_{LA} and J_{LA} from Cartesian coordinates (x, y) to polar coordinates (ρ, ϕ), to have the polar-mapped amplitude spectra I_{PLA} and J_{PLA} (Fig. 1(e)), respectively. Here, ϕ axis corresponds to the angle of polar coordinate system and ρ axis corresponds to the radius.

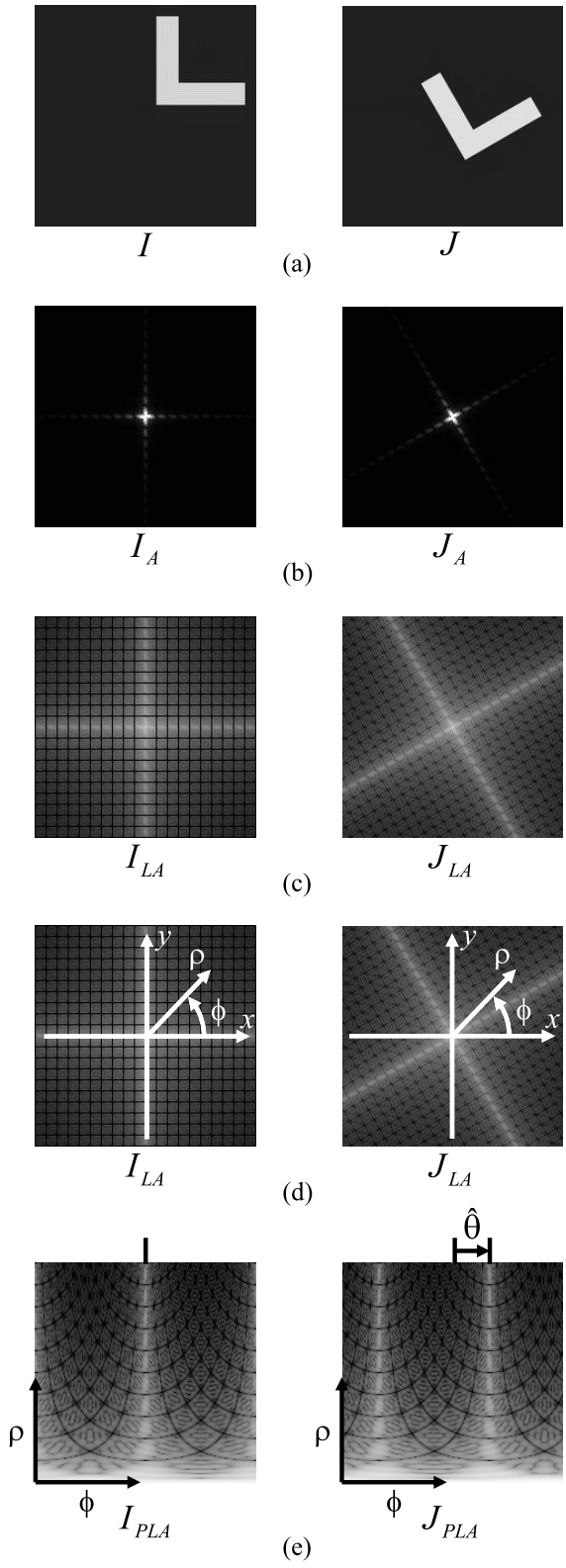

Fig. 1 Example of rotation estimation: (a) two input images, (b) amplitude spectra, (c) modified amplitude spectra, (d) polar coordinate system on the modified amplitude spectra, and (e) polar-mapped amplitude spectra.

Step 4:

Estimate the image displacement between I_{PLA} and J_{PLA} using their 2D POC function to obtain the rotation angle estimate $\hat{\theta}$. □

After the rotation estimation, we rotate back the second image J with the angle $-\hat{\theta}$ to obtain the rotation-normalized image J', and estimate the translation between I and J'. As a result, we can estimate the rotation angle and the translational displacement between I and J.

3. Rotation Estimation Algorithm Using 1D Phase-Only Correlation

As explained in the previous section, the image rotation between I and J is represented as the ϕ-axis image shift between the polar-mapped amplitude spectra I_{PLA} and J_{PLA}. In the conventional technique, major problems arise in Step 4, i.e., the use of 2D POC for angle estimation. For images with regular geometric patterns, signal energy is localized in certain spots in amplitude spectrum, exhibiting harmonic structure pattern in frequency domain. In other words, a considerable number of frequency components have only limited energy in its amplitude spectrum. In such a situation, even weak perturbation to the original image causes significant change in its amplitude spectrum, resulting in degraded accuracy in angle estimation. Figure 2 illustrates this situation where (a) shows the L-shaped pattern I and (c) shows its polar-mapped amplitude spectrum I_{PLA}. The spectrum shows the highly localized energy distribution, and large area of the spectrum contains only small signal amplitude. When small Gaussian white noise is added to the image as shown in (b), significant change of amplitude spectrum can be observed as shown in (d). This leads to significant degradation of estimation accuracy of rotation angle.

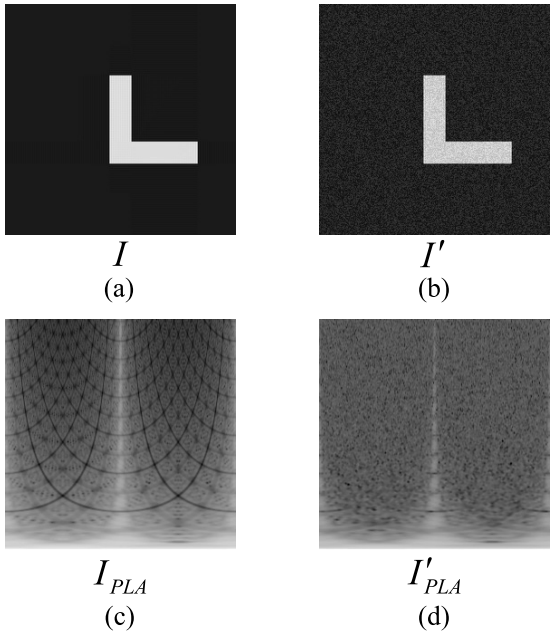

Fig. 2 Noise effects on the image with L-shaped pattern: (a) original image I, (b) noise-added version I' of the original image, (c) polar-mapped amplitude spectrum I_{PLA}, and (d) polar-mapped amplitude spectrum I'_{PLA}.

Addressing the problem, in our proposed method, we modify the Step 4 to estimate the displacement between I_{PLA} and J_{PLA} using 1D POC (presented in Sect. 3.1) with an adaptive line selection scheme. The conventional approach is to estimate the ϕ-axis displacement between I_{PLA} and J_{PLA} by 2D POC. In stead of using the whole image areas of I_{PLA} and J_{PLA}, we employ 1D POC on selected horizontal image lines (as illustrated in Fig. 3) for ϕ-axis displacement estimation. Major advantages of the proposed method are (i) significant reduction in computational complexity compared with the 2D approach, and (ii) improvement in estimation accuracy by adaptively selecting reliable image lines for 1D POC. In this section, first we introduce the principle of 1D POC and then present a high-accuracy rotation estimation algorithm using 1D POC.

3.1 1D Phase-Only Correlation

We propose a high-accuracy 1D translation estimation technique using 1D POC, which is a modification of the 2D-POC-based technique presented in [6] and includes a new method for performance improvement.

Consider two 1D signals, $f(n)$ and $g(n)$, where we assume that the index range is $n = -M, \cdots, M$ for mathematical simplicity, and hence the signal length is $N = 2M + 1$. (The discussion could be easily generalized to non-negative index ranges with power-of-two signal lengths.) Let $F(k)$ and $G(k)$ denote the Discrete Fourier Transforms (DFTs) of the two signals, which are given by

$$F(k) = \sum_{n=-M}^{M} f(n) W_N^{kn} = A_F(k) e^{j\theta_F(k)}, \tag{1}$$

$$G(k) = \sum_{n=-M}^{M} g(n) W_N^{kn} = A_G(k) e^{j\theta_G(k)}, \tag{2}$$

where $W_N = e^{-j\frac{2\pi}{N}}$. $A_F(k)$ and $A_G(k)$ are amplitude components, and $e^{j\theta_F(k)}$ and $e^{j\theta_G(k)}$ are phase components.

The normalized cross-power spectrum $R(k)$ is defined

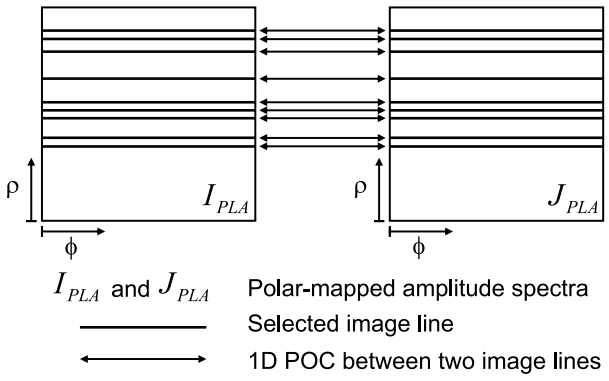

Fig. 3 Evaluating 1D POC only for selected image lines in polar-mapped amplitude spectra.

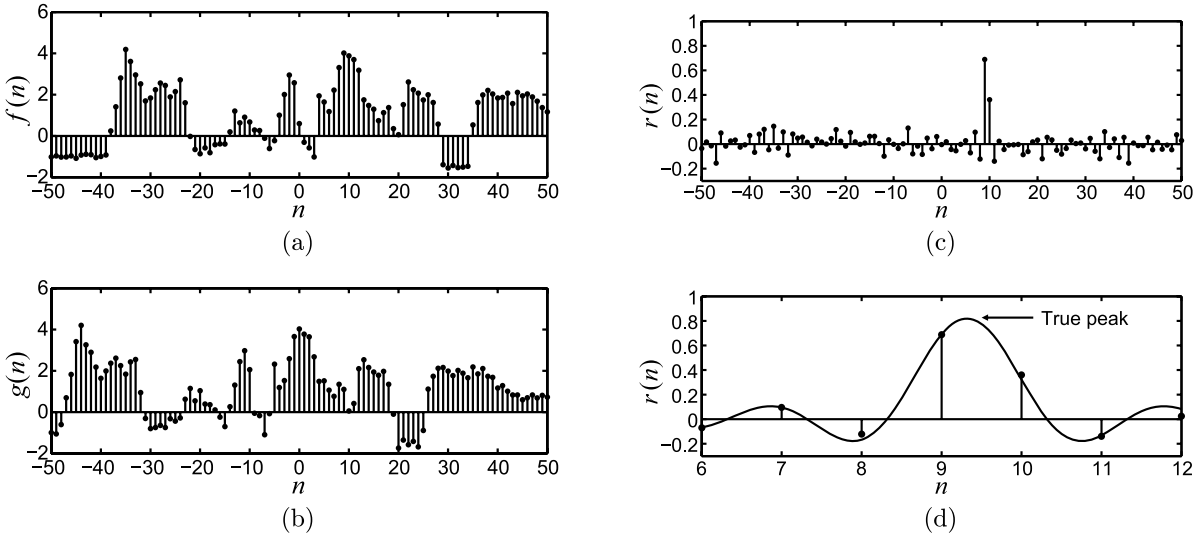

Fig. 4 Displacement estimation using 1D POC function: (a) original signal $f(n)$, (b) displaced version $g(n)$ of the original signal, (c) 1D POC function $r(n)$, and (d) function fitting for estimating the true peak position.

as

$$R(k) = \frac{F(k)\overline{G(k)}}{\left|F(k)\overline{G(k)}\right|} = e^{j\{\theta_F(k)-\theta_G(k)\}}, \tag{3}$$

where $\overline{G(k)}$ denotes the complex conjugate of $G(k)$. The POC function $r(n)$ is the Inverse Discrete Fourier Transform (IDFT) of $R(k)$ and is given by

$$r(n) = \frac{1}{N}\sum_{k=-M}^{M} R(k)W_N^{-kn}. \tag{4}$$

If the two signals $f(n)$ and $g(n)$ are similar, the POC function gives a distinct sharp peak. (When $f(n) = g(n)$, the POC function becomes the Kronecker delta function.) If not, the peak drops significantly. The height of the peak can be used as a good similarity measure for signal matching, and the position of the peak shows the translational displacement between the two signals. Figure 4 shows an example of the POC function, where (a) is an example signal and (b) is a displaced replica of the signal. Figures 4(c) and (d) are the corresponding POC function and its magnified view, respectively.

Now consider $f_c(x)$ as a signal defined in continuous space with a real-number index x. The displaced version of $f_c(x)$ can be represented as $f_c(x-\delta)$, where δ denotes small real-number displacement. Assume that $f(n)$ and $g(n)$ are spatially sampled signals of $f_c(x)$ and $f_c(x-\delta)$, and are defined as

$$f(n) = f_c(x)|_{x=nT}, \tag{5}$$

$$g(n) = f_c(x-\delta)|_{x=nT}, \tag{6}$$

where T is the sampling interval and the index range is given by $n = -M, \cdots, M$. For simplicity, we assume $T = 1$. In this case, normalized cross-power spectrum $R(k)$ and the POC function $r(n)$ between $f(n)$ and $g(n)$ can be approximated as

$$R(k) =\simeq e^{j\frac{2\pi}{N}k\delta}, \tag{7}$$

$$r(n) \simeq \frac{\alpha}{N}\frac{\sin\{\pi(n+\delta)\}}{\sin\left\{\frac{\pi}{N}(n+\delta)\right\}}, \tag{8}$$

where $\alpha = 1$. The above Eq. (8) represents the shape of the peak for the POC function between the same signals that are slightly displaced with each other. This equation gives a distinct sharp peak. The peak position $n = -\delta$ of the POC function corresponds to the displacement between the two signals. We can prove that the peak value α decreases (without changing the shape of the function itself), when small noise components are added to the original signals. Hence, we assume $\alpha \leq 1$ in practice. For signal (waveform) matching, we evaluate the similarity between the two signals by the peak value α, and estimate the displacement δ by the peak position.

We propose here some important techniques (A)–(D) for improving the accuracy of 1D signal matching. The techniques of (A)–(C) are the modification of their 2D version presented in [6] and (D) is a new method.

(A) Function fitting for high-accuracy estimation of peak position

We use Eq. (8) — the closed-form peak model of the POC function — directly for estimating the peak position by function fitting. By calculating the POC function, we can obtain a data array of $r(n)$ for each discrete index n. Figure 4(d) shows the POC function around the correlation peak, where the black dots indicate the discrete data values of $r(n)$. The solid line represents the estimated shape of the POC function. Thus, we can find the true position of the peak that may exist between sampling points by fitting the function of Eq. (8) to the calculated data array around the correlation peak, where α and δ are fitting parameters.

(B) Windowing to reduce boundary effects

Due to the DFT's periodicity, a 1D signal can be considered to "wrap around" at an edge, and therefore discontinuity, which is not supposed to exist in real world, occurs in DFT computations at the edges of 1D signals. We reduce the effect of a discontinuity at a signal border by applying a window function to the input signals $f(n)$ and $g(n)$. For example, we can employ a Hanning window defined as

$$w(n) = \frac{1 + \cos\left(\frac{\pi n}{M}\right)}{2}. \quad (9)$$

(C) Spectral weighting for reducing aliasing and noise effects

In ordinary situation, high frequency components may have less reliability (low S/N) compared with the low frequency components. We could improve the estimation accuracy by applying a low-pass-type weighting function $H(k)$ to $R(k)$ in frequency domain and eliminating high frequency components with low reliability. One of the simplest weighting functions is defined as

$$H(k) = \begin{cases} 1 & |k| \le U \\ 0 & \text{otherwise} \end{cases}, \quad (10)$$

where U is an integer satisfying $0 < U \le M$. The normalized cross-power spectrum $R(k)$ is multiplied by the weighting function $H(k)$ when calculating the 1D IDFT in Eq. (4). Then the modified $r(n)$ will be given by

$$r(n) \simeq \frac{\alpha}{N} \cdot \frac{\sin\{\frac{V}{N}\pi(n+\delta)\}}{\sin\{\frac{\pi}{N}(n+\delta)\}}, \quad (11)$$

where $V = 2U + 1$. In our experiments, we choose $U = \lfloor M/2 \rfloor$. When using the spectral weighting technique, Eq. (11) should be used for function fitting instead of Eq. (8).

(D) Averaging 1D POC function to improve peak-to-noise ratio

When image quality is poor, a single 1D POC function is not sufficient for estimating accurate displacement estimation due to degraded Peak-to-Noise Ratio (PNR). We can improve PNR by averaging a set of 1D POC functions. Given B distinct 1D image signals $f_i(n)$ $(i = 1, 2, \cdots, B)$, and $g_i(n)$ $(i = 1, 2, \cdots, B)$. Then, we compute the B distinct 1D POC functions $r_i(n)$ between $f_i(n)$ and $g_i(n)$. By taking the average of $r_i(n)$ for $i = 1, 2, \cdots, B$, we have the overall correlation surface $r(n)$ with significantly improved PNR.

3.2 High-Accuracy Rotation Estimation Algorithm Using 1D POC

The proposed algorithm consists of two procedures as shown in Fig. 5: (i) adaptive line selection and (ii) rotation estimation using 1D POC. In the adaptive line selection procedure (i), the system finds reliable image lines automatically by analyzing the registered reference image I in advance. In typical situation of industrial machine vision, the length of time taken to register the reference image in the system is not limited, so we can use enough time to perform procedure (i). The system first generates a new image I' by rotating the reference image I by the angle Θ, and computes their polar-mapped amplitude spectra I_{PLA} and I'_{PLA}. The next step is to compute the 1D POC function for every pair of horizontal image lines between I_{PLA} and I'_{PLA} and to estimate rotation angles for all line pairs. Then, the system selects the reliable image lines for which the estimated angles are close in value to the true angle Θ. This procedure is performed only once when the reference image I is registered in the system. So, the cost of rotation estimation is not affected by the procedure (i). In the rotation estimation procedure (ii), on the other hand, the system estimates the rotation angle between I and J using the selected image lines in I_{PLA} and J_{PLA}. The followings are detailed procedures.

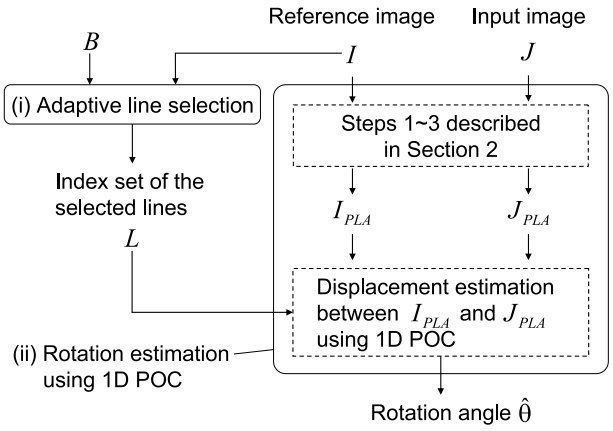

Fig. 5 Flow diagram of the proposed algorithm.

(i) Adaptive line selection

Input:

- the reference image I to be registered in the system
- the positive integer B, representing the number of reliable image lines to be selected

Output:

- the index set L of selected image lines

Step 1:

Generate the image I' by rotating the reference image I by the angle Θ, where $\Theta = 30$ [degree] in our experiments. Calculate the polar-mapped amplitude spectra I_{PLA} and I'_{PLA} from I and I', respectively.

Step 2:

Let i be the index of horizontal image lines.
For all i:

- Extract the ith image lines from I_{PLA} and I'_{PLA}. Evaluate the 1D POC function between the lines and estimate the displacement $\hat{\theta}_i$ and the peak value $\hat{\alpha}_i$.
- Compare $\hat{\theta}_i$ with Θ to verify the reliability of the ith image lines. If $|\hat{\theta}_i - \Theta| \le \epsilon_{th}$, add the index i to the set L as an effective line index, where ϵ_{th} is a certain threshold value.

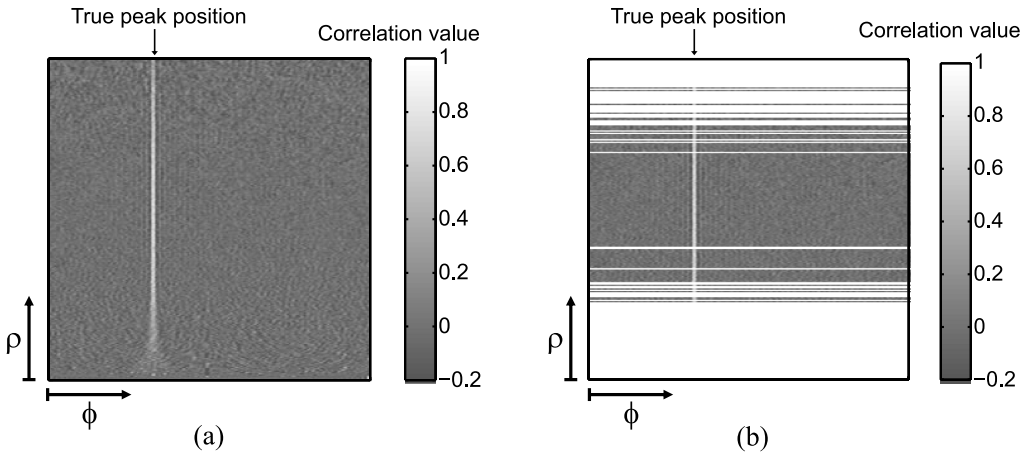

Fig. 6 Examples of 1D POC functions: (a) for all image lines, and (b) for selected image lines.

Step 3:

Let $|L|$ denote the number of elements in the set L. Sort the indices in L according to their correlation value $\hat{\alpha}_i$ in descending order. If $|L| \geq B$, select the top B indices in L and update L. On the other hand, if $|L| < B$, we set $L = \emptyset$, where $\emptyset$ represents the empty set. □

In this procedure, we can obtain a set of effective image lines for rotation estimation. Figures 6(a) and (b) show examples of 1D POC functions for all image lines and only for the lines selected by the above procedure, respectively. In Fig. 6(a), the number of image lines is 256 and in Fig. 6(b), the number of selected image lines is B = 128. From the careful observation of the POC functions in Fig. 6(a), we can classify the POC functions into three types using their peak: (1) the peak value is high but the peak position is wrong, (2) the peak position is correct but the peak value is low, and (3) the peak position is correct and the peak value is high. Here, the types (1) and (2) give unreliable lines, and the type (3) gives reliable lines. The use of adaptive line selection described the above makes possible to remove all unreliable lines and select the lines exhibiting true peaks as shown in Fig. 6(b).

(ii) Rotation estimation using 1D POC

Inputs:

- the reference image I to be registered in the system
- the input image J for which the rotation angle is estimated with respect to the reference image I
- the index set $L(\neq \emptyset)$ of selected image lines

Output:

- the estimated rotation angle $\hat{\theta}$ of J with respect to I

Step 1:

Calculate the polar-mapped amplitude spectra I_{PLA} and J_{PLA} from I and J, respectively.

Step 2:

For all $i \in L$, extract the ith image lines from I_{PLA} and J_{PLA} and compute the 1D POC function between the lines.

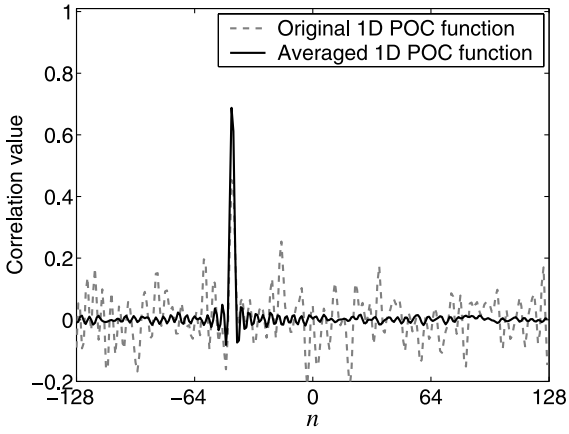

Fig. 7 Averaging 1D POC function to improve Peak-to-Noise Ratio (PNR).

Step 3:

Calculate average of 1D POC functions obtained from Step 2. Estimate the displacement $\hat{\theta}$ between I_{PLA} and J_{PLA} using the averaged 1D POC function. □

In this procedure, we employ the averaged 1D POC function to estimate the ϕ-axis displacement between I_{PLA} and J_{PLA} proposed in Sect. 3.1(D). By using the averaged 1D POC function, we can significantly improve PNR. Figure 7 shows an example of PNR improvement through averaging. After the averaging, we apply the function fitting technique (described in Sect. 3.1) for estimating the true peak position and height.

4. Experiments and Discussions

This section describes a set of experiments for evaluating the accuracy of the proposed algorithm. In the experiments, we estimate the rotation angle between two images taken by a CCD camera (View Plus SCOR-14SOM-CS with μTRON FV1520 lens). The target object is mounted on a micro stage that allows precise rotation as shown in Fig. 8. We employ two different types of images: one is the wood-texture image

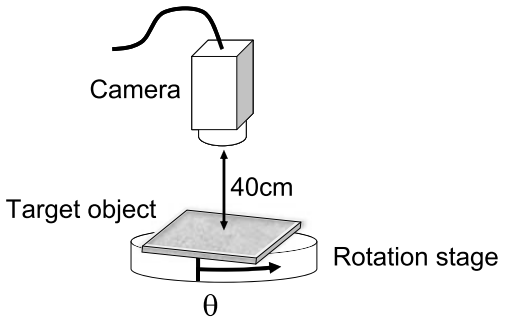

Fig. 8 Experimental system setup.

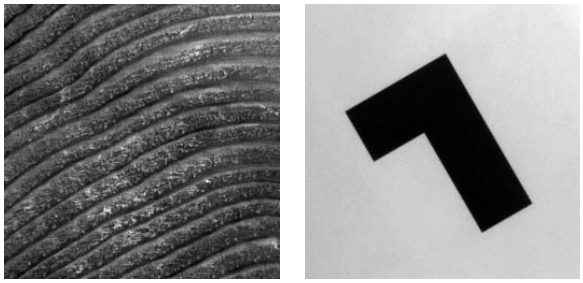

Fig. 9 Examples of captured images: (a) wooden texture and (b) artificial geometric pattern.

shown in Fig. 9(a) and the other is the artificial geometric pattern shown in Fig. 9(b). The distance between the camera and the object is 40 cm. The image size is 256×256 pixels. We have rotated the micro stage from 0 to 90 degrees with each step of 1 degrees, and estimated the rotation angle between a reference image before moving the target object and each image after moving it.

In many industrial applications, the target object does not have to be stationary state so that the captured image is blurred or smeared. To reduce such undesirable effects, the system sets exposure time of CCD camera short. And, the system also employs the short exposure time setting due to the limitation of total processing time. To simulate such situations, we have taken five images with five different exposure times 1 ms, 3 ms, 6 ms, 10 ms and 40 ms at each step of the rotation stage.

We compare the proposed rotation estimation algorithm (described in Sect. 3) with the 2D POC-based rotation estimation algorithm (described in Sect. 2). The estimation error in the rotation angle is evaluated by

$$\varepsilon_i = \hat{\theta}_i - \theta_i,$$

where $\hat{\theta}_i$ [degree] and θ_i [degree] are the estimated angle and the actual angle of the rotation stage for the ith micro step, respectively.

Table 1 summarizes the error in rotation estimation for two target objects, where RMS error represents *Root Mean Square* error. We observe that the estimation error increases as the image quality decreases (i.e., as the exposure time decreases). As for the wooden texture, the estimation accuracy is similar for both methods "2D POC" and "1D POC," where "2D POC" corresponds to 2D POC-based rotation estimation algorithm and "1D POC" means 1D POC-based rotation estimation algorithm. As for the geometric pattern, the estimation accuracy of "1D POC" is significantly higher than that of "2D POC." For images with regular geometric patterns, signal energy is localized in certain spots in amplitude spectrum. The estimation accuracy of "2D POC" is low, since the whole image areas of the polar-mapped amplitude spectra are used for rotation estimation. On the other hand, the estimation accuracy of "1D POC" is high, since only the effective horizontal image lines in the polar-mapped amplitude spectra are used for rotation estimation. By comparison the results of Tables 1 (a) and (b), result (a) exhibits better rotation estimation performance than result (b). This reason is that the signal energy of the wooden texture is distributed in large areas in amplitude spectrum, so the effective region for rotation estimation is larger than that of the geometric pattern.

Table 1 Error [degree] in rotation estimation.

(a) Wooden texture

	RMS error		Maximum error	
Exposure time	2D POC	1D POC	2D POC	1D POC
1 ms	0.123	0.111	0.285	0.303
3 ms	0.041	0.037	0.105	0.101
6 ms	0.037	0.030	0.128	0.091
10 ms	0.030	0.025	0.091	0.068
40 ms	0.025	0.021	0.062	0.055

(b) Geometric pattern

	RMS error		Maximum error	
Exposure time	2D POC	1D POC	2D POC	1D POC
1 ms	33.378	0.274	127.525	0.706
3 ms	20.302	0.092	112.410	0.243
6 ms	0.150	0.077	0.468	0.218
10 ms	0.099	0.055	0.349	0.185
40 ms	0.043	0.034	0.115	0.095

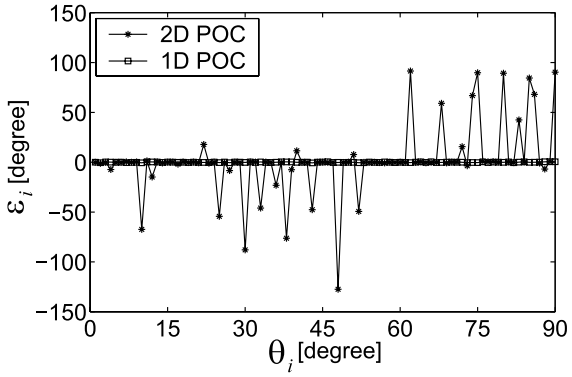

Fig. 10 Error in rotation estimation for the L-shaped geometric pattern with the exposure time 1 ms.

Figure 10 shows error in rotation estimation, where the target object is geometric pattern and the exposure time is 1 ms. The horizontal axis represents the actual angle θ_i [degree] of the rotation stage, and the vertical axis represents the error ε_i in rotation estimation. We can see that the con-

Table 2 RMS error [degree] when changing the number of selected lines B.

(a) Wooden texture

	Exposure time				
B	1 ms	3 ms	6 ms	10 ms	40 ms
20	7.777	0.057	0.037	0.039	0.027
40	0.148	0.047	0.039	0.032	0.025
60	0.126	0.046	0.033	0.027	0.024
80	0.123	0.043	0.032	0.027	0.023
100	0.121	0.039	0.031	0.026	0.022
120	0.124	0.037	0.030	0.026	0.022
140	0.118	0.037	0.032	0.025	0.022
160	0.111	0.037	0.031	0.026	0.021
180	0.113	0.037	0.032	0.027	0.022
200	0.114	0.037	0.032	0.028	0.022
220	0.117	0.040	0.035	0.029	0.023

(b) Geometric pattern

	Exposure time				
B	1 ms	3 ms	6 ms	10 ms	40 ms
20	36.7660	20.528	9.388	0.131	0.062
40	35.8180	12.977	0.111	0.107	0.050
60	28.0744	15.738	0.097	0.080	0.046
80	26.7065	0.127	0.086	0.067	0.041
100	24.6344	0.108	0.090	0.062	0.038
120	20.9152	0.104	0.084	0.057	0.036
140	18.3557	0.092	0.081	0.056	0.035
160	15.7324	0.093	0.079	0.057	0.034
180	0.2764	0.093	0.079	0.057	0.036
200	0.2934	0.093	0.077	0.055	0.037
220	0.3033	0.106	0.082	0.068	0.043

ventional algorithm "2D POC" fails in some θ_i. On the other hand, the proposed algorithm "1D POC" can estimate the rotation angle accurately for all θ_i. As is observed in the above results, the proposed algorithm exhibits high performance compared with the conventional algorithm.

The number of effective lines B in our proposed algorithm is selected by experimental optimization as shown in Table 2. By changing the parameter B we can reduce the estimation error. From Table 2, the better results are obtained when the number of lines B is around 120–200.

We evaluate the computation cost required for estimating a rotation angle. In our proposed algorithm, the procedure (i) adaptive line selection is performed only once when the reference image I is registered in the system. So, we do not include the computational cost of this procedure. The cost for computing the polar-mapped amplitude spectrum I_{PLA} is also not included in the total computational cost because of the same reason. We assume that the image size is 256×256 and the number of selected lines B is 128.

Table 3 summarizes the number of operations for estimating the rotation angle between two images, where "ADD," "MUL," "DIV," "SQRT" and "LOG" denote the number of additions, multiplications, divisions, square roots and logarithms, respectively. By using the proposed method, significant reduction in computational cost is expected in comparison with conventional method, where the number of operations can be reduced to 50%. As is observed in the above experiments, the proposed algorithm makes possible to improve the accuracy of rotation estimation and to reduce the computational cost.

Table 3 Number of operations for estimating a rotation angle.

	2D POC	1D POC	Ratio = $\frac{\text{1DPOC}}{\text{2DPOC}}$
ADD	10,289,170	4,429,842	43%
MUL	7,143,438	3,084,302	43%
DIV	262,146	131,074	50%
SQRT	131,072	65,536	50%
LOG	65,536	32,768	50%

5. Conclusion

This paper has presented a technique for image rotation estimation based on 1D Phase-Only Correlation (POC). The use of 1D POC in rotation estimation makes possible to improve the estimation accuracy as well as to reduce the computational cost compared with the conventional 2D POC-based algorithm. For our future work, we will implement the proposed algorithm on practical vision sensors and evaluate the performance of our algorithm.

References

[1] L.G. Brown, "A survey of image registration techniques," ACM Computing Surveys, vol.24, no.4, pp.325–376, Dec. 1992.
[2] B. Zitova and J. Flusser, "Image registration methods: A survey," Image Vis. Comput., vol.21, no.11, pp.977–1000, Oct. 2003.
[3] C.D. Kuglin and D.C. Hines, "The phase correlation image alignment method," Proc. Int. Conf. Cybernetics and Society, pp.163–165, 1975.
[4] E.D. Castro and C. Morandi, "Registration of translated and rotated images using finite Fourier transforms," IEEE Trans. Pattern Anal. Mach. Intell., vol.9, no.5, pp.700–703, Sept. 1987.
[5] Q. Chen, M. Defrise, and F. Deconinck, "Symmetric phase-only matched filtering of Fourier-Mellin transforms for image registration and recognition," IEEE Trans. Pattern Anal. Mach. Intell., vol.16, no.12, pp.1156–1168, Dec. 1994.
[6] K. Takita, T. Aoki, Y. Sasaki, T. Higuchi, and K. Kobayashi, "High-accuracy subpixel image registration based on phase-only correlation," IEICE Trans. Fundamentals, vol.E86-A, no.8, pp.1925–1934, Aug. 2003.
[7] http://www.aoki.ecei.tohoku.ac.jp/research/poc.html
[8] M. Morikawa, A. Katsumata, and K. Kobayashi, "Pixel-and-column pipeline architecture for FFT-based image processord," Proc. 2002 IEEE Int. Symp. on Circuits and Systems, pp.687–690, May 2002.

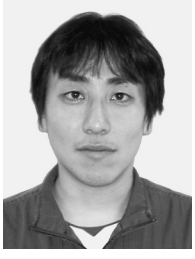

Sei Nagashima received the B.E. degree in information engineering and the master degree of information sciences from Tohoku University, Sendai, Japan, in 2003 and 2005, respectively. He is currently working toward the Ph.D. degree at Tohoku University. His research interests include signal and image processing.

Koichi Ito received the B.E. degree in electronic engineering, and the M.S. and Ph.D. degree in information sciences from Tohoku University, Sendai, Japan, in 2000, 2002 and 2005, respectively. He is currently an Assistant Professor of the Graduate School of Information Sciences at Tohoku University. From 2004 to 2005, he was a Research Fellow of the Japan Society for the Promotion of Science. His research interest includes signal and image processing, and biometric authentication.

Takafumi Aoki received the B.E., M.E., and D.E. degrees in electronic engineering from Tohoku University, Sendai, Japan, in 1988, 1990, and 1992, respectively. He is currently a Professor of the Graduate School of Information Sciences at Tohoku University. For 1997–1999, he also joined the PRESTO project, Japan Science and Technology Corporation (JST). His research interests include theoretical aspects of computation, VLSI computing structures for signal and image processing, multiple-valued logic, and biomolecular computing. Dr. Aoki received the Outstanding Paper Award at the 1990, 2000, 2001 and 2006 IEEE International Symposiums on Multiple-Valued Logic, the Outstanding Transactions Paper Award from the Institute of Electronics, Information and Communication Engineers (IEICE) of Japan in 1989 and 1997, the IEE Ambrose Fleming Premium Award in 1994, the IEICE Inose Award in 1997, the IEE Mountbatten Premium Award in 1999, the Best Paper Award at the 1999 IEEE International Symposium on Intelligent Signal Processing and Communication Systems, the IP Award at the 7th LSI IP Design Award in 2005, and the Best Paper Award at the 14th Workshop on Synthesis And System Integration of Mixed Information technologies.

Hideaki Ishii received the B.E. degree in electronic engineering from Tokyo University of Science, Noda, Chiba, Japan, in 1986. He is currently a manager of Project Sect. 4, Product Development Department, Advanced Automation Company, Yamatake Corporation, Fujisawa, Japan. His general interests includes CMOS image sensor, and two-dimensional sensing.

Koji Kobayashi received the B.E. and M.E. degrees in electronic engineering from Tohoku University, Sendai, Japan, in 1976, and 1978, respectively. He is currently a general manager of Vision Sensing Department, Yamatake Corporation, Fujisama, Japan. His general interests includes real-time automation system architecture, network communication protocol LSI, biometric image processing, CMOS image sensor, and three-dimensional sensing.